Eur. Phys. J. B **12**, 23–30 (1999)

THE EUROPEAN PHYSICAL JOURNAL B

EDP Sciences

Mutual inductance effects in rf driven planar Josephson junctions arrays

G. Filatrella,[1] A. Petraglia[2,a] and G. Rotoli[3]

[1] Unità INFM Salerno and Facoltà di Scienze, Via Caio Ponzio Telesino 11, Università del Sannio, 82100 Benevento, Italy
[2] Unità INFM and Dipartimento di Fisica, Università di Salerno, 84081 Baronissi (SA), Italy
[3] Unità INFM and Dipartimento di Energetica, Università di L'Aquila 67010 Località Monteluco-Roio Poggio (AQ), Italy

Received 9 November 1998 and Received in final form 6 April 1999

Abstract. In this paper we investigate the behavior of moderate size two-dimensional classical arrays of Josephson junctions in presence of an external oscillating field. We have included in the model the effects due to mutual inductance terms, and we have employed an explicit set of differential equations. We have found that the discretization parameter $\beta_{\rm L}$ – *i.e.* the coupling term due to the inductance of the loops – is the most important parameter to determine the height of the Shapiro steps for a given amplitude and frequency of the rf-bias. The amplitude of the Shapiro steps in the case of zero frustration as a function of the coupling term shows a remarkable minimum for intermediate values when we retain all terms of the full model with mutual inductances, while the limits for very large and very small values of $\beta_{\rm L}$ they are the same of the single Josephson junction. For the case of frustration 1/2 the Shapiro step becomes smaller in the rigid limit (*i.e.*, small $\beta_{\rm L}$) as expected for the XY model, and tends to the limit value of the single junctions for the decoupled case (*i.e.*, large $\beta_{\rm L}$).

PACS. 85.25.Am Superconducting device, characterization, design, and modeling – 85.25.Dq Superconducting logic elements and memory devices

1 Introduction

Planar arrays of small Josephson junctions driven by a rf bias current have been extensively investigated both for applications and for a deeper understanding of the properties of nonlinear oscillators. Indeed, rf-induced states such as Shapiro steps have been observed. They appear as horizontal branches in the current voltage (IV) curves at voltages $nN_{\rm r}h\nu/2qe$ (n and q are integers, h is the Planck constant, ν is the frequency of the applied radiation, e is the elementary charge, $N_{\rm r}$ is the number of rows of the array). These steps are usually classified according to the integers n and q. The behavior is much richer than that observed in single Josephson junctions, suggesting that a new, and presumably more complicated, mechanism is at work in the underlying dynamics [1–3].

Giant Shapiro steps appear at the fundamental frequency ($n = 1$, $q = 1$) in zero external field and can be ascribed to collective modes whose dynamics is closely related to the single junction dynamics: each junction exactly follows the rf drive. Subharmonic Shapiro steps ($n = 1$ and any q) appear also in zero field, and the origin is known to be due to boundary effects [4]. Fractional Shapiro steps (any n and $q > 1$), finally, arise in presence of magnetic field only; they are due to the commensurability between the pattern of vortices induced by the fields and the array [5].

The difficulties to investigate two-dimensional arrays can be grouped in three classes:

- An analytical insight is very difficult if the coupling due to the inductance is included: The resulting model is a set of coupled ordinary differential equations that has not a simple structure. The most important results have been obtained for the cases in which the dynamics can be reduced to that of simpler systems, such as SQUIDs, square four junction cells, and single junctions [4,6].
- The integration time for numerical investigation increases rapidly with the size of the array. Various approximations have been proposed to simplify the problem. The most used approximation has been the zero inductance limit (the so called XY model, for a discussion see Ref. [7]), and the more sophisticated nearest neighbor inductance models (NS model [8]).
- The large number of parameters in the model makes difficult the exhaustive exploration of the dynamics and the understanding of the general behavior of the array.

In spite of the difficulties, some understanding has been gained. It has been proved that zero field subharmonic steps arise from collective behavior [5,9,10].

[a] e-mail: petra@physics.unisa.it

Moreover, the arrays have been shown to behave like small inductance SQUIDs when the applied rf current amplitude becomes large [11]; the relevant parameters are the critical currents of the junctions perpendicular to the bias and the equivalent inductance's of the junctions. Numerical simulations have also shown that for large arrays subharmonic steps disappear [3]. Giant and Fractional Shapiro steps have also been extensively investigated and the behavior of the steps height versus the rf current amplitude have been found in various limits [3,11] (see also Marino [12] for the high frequency limit).

Many investigations have been carried out in the zero inductance limit, *i.e.* neglecting the effects of the field generated by the currents (XY models), or at most including only the field generated in the nearest loop (Nakajima-Sawada model, NS [8]). In recent years, however, it has become clear the importance of self-field effects; approaches with the full inductance matrix have been proposed and new types of dynamics have been shown to arise [7,13–15]. For the rf driven case, SQUIDs have been studied including the inductance effects [11,16]. In particular Vanneste *et al.* [16] have shown, both experimentally and numerically, how the voltage *versus* magnetic field characteristics of an overdamped SQUID with rf bias current depends upon the inductance parameter.

In this paper we will use an approach to the modeling of the full mutual inductance effects in planar arrays that results in an explicit set of differential equations; such approach was also proposed by Phillips *et al.* [15] but an implicit method was used to investigate large array sizes. Here we will use the explicit method because for relatively small array size (see the discussion in Sect. 2) it significantly shorts the computing time. We will investigate the behavior of the locking range versus the self-inductance parameter $\beta_{\rm L}$. In doing so we extend some previous results obtained by Phillips *et al.* [15] to larger $\beta_{\rm L}$ values. To gain a deeper insight of the underlying dynamics we will show the cases in which the dynamics can be explained in terms of dynamics of simpler systems and point out regions in which the self-field generates internal modes. Since the internal motion of fluxons in rf-induced steps in presence of frustration has been numerically investigated by reference [5] and experimentally with the LTSEM analysis [17], for frustrated arrays we will concentrate on the overall behavior of the amplitude of the steps and we will not show studies of the internal dynamics.

The paper is organized as follows: in Section 2 we will describe how we have included mutual inductance terms and we will give the set of the simulated equations. In Section 3 we will focus on the Shapiro steps and give some analytical results for their amplitude. In Section 4 we will show the results of numerical simulations to check the analytical predictions and to investigate the system outside the region of parameters where analytical predictions are expected to work. The results will be summarized in Section 5.

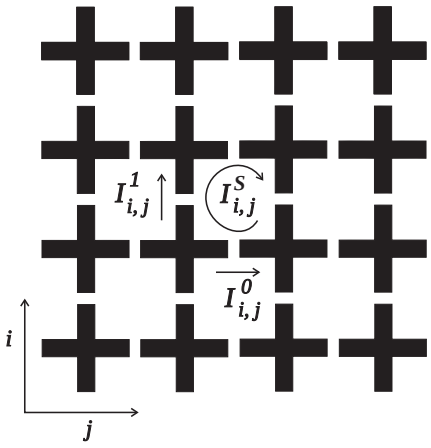

Fig. 1. A schematic view of the two-dimensional array. The gap between the thick lines represents a Josephson junction. The bias current is injected parallel to the i direction.

2 A model for the array with mutual inductance terms

In the following we will use a set of $N_{\rm r} \times N_{\rm c}$ *explicit* equations (where $N_{\rm r}$ is the number of vertical junctions in each row of the array and $N_{\rm c}$ is the number of horizontal junction in each column), retaining all the mutual inductance terms. For completeness, we show in detail how we have included the mutual inductance terms. This derivation follows the derivation of reference [15], a somewhat different derivation of the same explicit scheme can be found in [18]. Domínguez and José have shown how the equations depend on the choice of the gauge; the equations used in this paper correspond to the temporal gauge [5]. A schematic drawing of a two-dimensional plane array is shown in Figure 1: the thick lines are the superconductors, the gaps represent the junctions. In the following we suppose all the junctions to be identical. To derive the equations, we first compute the current across a branch $I^{\rm b}_{i,j}$ in terms of the Josephson relation between the phase across the junctions, $\varphi_{i,j}$; normalizing the current respect to the critical current of the junctions I_0 and the time respect to $\hbar/2eRI_0$ (R is the normal resistance of the junctions due to the quasiparticle tunneling) and in the overdamped limit, the current reads [19]

$$I^k_{i,j} = \sin\varphi^k_{i,j} + \dot{\varphi}^k_{i,j}. \tag{1}$$

The indices $i = 1, ..., N_{\rm r}$ and $j = 1, ..., N_{\rm c}$ denote the mesh; k indicates the direction of the branch, horizontal ($k = 0$) or vertical ($k = 1$). Here, $\sin\varphi^k_{i,j}$ is the current through the Josephson element, and $\dot{\varphi}^k_{i,j}$ is the current through a resistor that mimics the quasi-particle terms. To satisfy the Kirchhoff law for the currents in each node we define the mesh currents $I^s_{i,j}$ connected to the branch currents by the relationship (see Fig. 1):

$$I^k_{i,j} = \delta_{1,k}\left(I^s_{i,j} - I^s_{i,j-1} + \gamma\right) + \delta_{0,k}\left(I^s_{i-1,j} - I^s_{i,j}\right). \tag{2}$$

$\delta_{i,j}$ is the Kronecker operator, γ denotes the normalized bias current injected in the top nodes and extracted from the bottom nodes, this choice being similar to that referred as i) in Appendix C by Domínguez and José [20]. As noted in the latter paper, this choice is irrelevant when all mutual inductances are included because all choices lead to the same physical result, but this particular choice is the most convenient to compare the effect of full mutual inductance models with truncated matrix models. If there is an *ac* bias added to the *dc* bias, the current term γ can be written as:

$$\gamma = \gamma_{\rm dc} + \gamma_{\rm rf}\cos(\omega t). \tag{3}$$

It is more convenient to introduce the vectors $\mathbf{I}^{\rm b}$ (whose components are the branch currents $I^k_{i,j}$, the LHS of equation (2)), $\mathbf{I}^{\boldsymbol{s}}$ (whose components are the mesh currents $I^s_{i,j}$) and $\boldsymbol{\gamma}$ (whose component are γ in correspondence of a vertical junction and 0 otherwise). With the help of these vectors one can rewrite in a matrix form equations (2,3):

$$\mathbf{I}^{\rm b} = \hat{K}\mathbf{I}^{\boldsymbol{s}} + \boldsymbol{\gamma} \tag{4}$$

The fluxoid quantization rule for each mesh gives another set of equations, one for each mesh:

$$\Sigma\varphi = \frac{2\pi}{\Phi_0}\phi^{\rm TOT} = \frac{2\pi}{\Phi_0}\left(\phi^{\rm ext} + \phi^{\rm induced}\right) \tag{5}$$

where the sum Σ spans over the junctions of a mesh, $\phi^{\rm TOT}$ is the total flux in the mesh due to the external flux ($\phi^{\rm ext}$) and to the field induced by the currents flowing in all meshes of the array ($\phi^{\rm induced}$). Normalizing the flux respect to the elementary flux quantum $\Phi_0 = h/2e$ and with the use of the SQUID parameter $\beta_{\rm L} = 2\pi L' I_0/\Phi_0$ (L' is the self-inductance of the SQUID), equation (5) can be rewritten in a matrix form as:

$$\hat{M}\boldsymbol{\varphi} = 2\pi\mathbf{f} + \beta_{\rm L}\hat{L}\mathbf{I}^s + \beta_{\rm L}\hat{\Gamma}\boldsymbol{\gamma} \tag{6}$$

where $\hat{M}$ performs the sum of the phases around a mesh, *i.e.* the left hand side of equation (5), $\mathbf{f}$ is a vector that represents the normalized external field in each mesh (frustration). The last two terms are the contributions to the induced flux due to the current $\mathbf{I}^s$ and the bias currents $\boldsymbol{\gamma}$ in all the meshes of the array. These contributions are introduced *via* the matrices (normalized to the self inductance of the plaquette, L') $\hat{L}$ and $\hat{\Gamma}$, that we therefore shall call the mutual inductance matrices. An expression for such matrices will be calculated below. equation (6) can be easily inverted to give explicitly, with the help of equation (4), the dependence of the branch currents as a function of the phases:

$$\mathbf{I}^{\rm b} = \hat{K}\left[-\frac{1}{\beta_{\rm L}}\hat{L}^{-1}\left(\hat{M}\boldsymbol{\varphi} - 2\pi\mathbf{f}\right) - \hat{L}^{-1}\hat{\Gamma}\boldsymbol{\gamma}\right] + \boldsymbol{\gamma}, \tag{7}$$

that together with equation (1) gives a set of explicit differential equations.

If one retains only self-inductance terms the matrix $\hat{L}$ reduces to unity and the vector $\hat{\Gamma}\boldsymbol{\gamma}$ vanishes. This corresponds to the NS approximation [8], sometimes referred as the nearest neighbors approximation. Equation (7) can be integrated directly and does not require to invert a matrix at each time step as in other schemes [5,15] and thus cuts down the computing time. Still to apply the matrix $\hat{L}^{-1}\hat{M}$ to the vector $\boldsymbol{\varphi}$ is the most time-consuming task, requiring $O((N_{\rm r}\times N_{\rm c})^2)$ operations for each time step, in contrast to the NS algorithm, or any truncation of the matrix $\hat{L}$, that requires only $O(N_{\rm r}\times N_{\rm c})$ operations. The time to invert the matrix at the beginning of the computation is in this scheme completely irrelevant, in contrast to the implicit algorithms [15]. On the other hand implicit schemes can be significantly accelerated for large $N_{\rm r}\times N_{\rm c}$ exploiting the symmetry of the matrix $\hat{L}$: It is possible to employ Fast Fourier Transform routines for matrix multiplication, that require only $O([N_{\rm r}\times N_{\rm c}]\log_2[N_{\rm r}\times N_{\rm c}])$ operations. Unfortunately, these routines must be repeated, $10-20$ times to converge [20,21], thus making implicit schemes slower than the integration of the explicit equations for relatively small $N_{\rm r}\times N_{\rm c}$ (up to $N_{\rm r}\times N_{\rm c}\simeq 100$). Thus we have preferred to use the explicit method, although it has the additional disadvantage to require larger memory storage (of the order of $(N_{\rm r}\times N_{\rm c})^2$).

To write explicitly the matrix $\hat{L}$ it is necessary to compute the mutual inductance between two loops 1 and 2:

$$L_{1,2} = \frac{1}{L' a_i a_j}\frac{\mu_0}{4\pi}\int_{a_i}\int_{a_j}\oint_1 {\rm d}\boldsymbol{s}_1\cdot\oint_2\frac{{\rm d}\boldsymbol{s}_2}{r_{1,2}}{\rm d}a_i{\rm d}a_j \tag{8}$$

where ${\rm d}\boldsymbol{s}_{1,2}$ are elements of the circuit parallel to the axis of the wires; the variable $r_{1,2}$ is the distance between them. The variables $a_{i,j}$ are the conductor cross section areas. This expression clearly diverges if the loops coincide; in this case the well-known formulas for self-inductance can be used, the formula actually used depends in detail upon the geometry of the wires, for a square loop with cylindrical wires the self-inductance is given by [22]:

$$L' = \frac{2\mu_0 R}{\pi}\left[\ln\left(\frac{2R}{a(1+\sqrt{2})}\right) + a/R + \sqrt{2} - 2\right], \tag{9}$$

where R is the length of the branches, and a is the radius of the wires. For a square washer it reads instead [23]:

$$\tilde{L} = \frac{2\mu_0 R}{\pi}\left[1.15\ln\left(\frac{a/R + 0.096}{a/R}\right) + 1.96\right] \tag{10}$$

where again R is the branch length, and a is the washer width. In this work we have extensively used equation (9), but we have also checked with equation (10) that the results do not change qualitatively.

To compute the other terms of the mutual inductance matrix we note that $\hat{L} = \hat{M}\hat{L}_{\rm b}\hat{M}^{\rm T}$ and $\hat{\Gamma} = \hat{M}\hat{L}_{\rm b}$ where $\hat{L}_{\rm b}$ is the branch-branch inductance matrix. So the loop-loop integral can be divided in the branch-branch parts. We have assumed an uniform distribution of the currents in the film and, moreover, we have assumed the current to flow in filamentous wires ($a\to 0$; this is a good approximation in most practical cases as shown in Ref. [24]). The matrix $\hat{L}$ will not change significantly for $R/a \gg 1$,

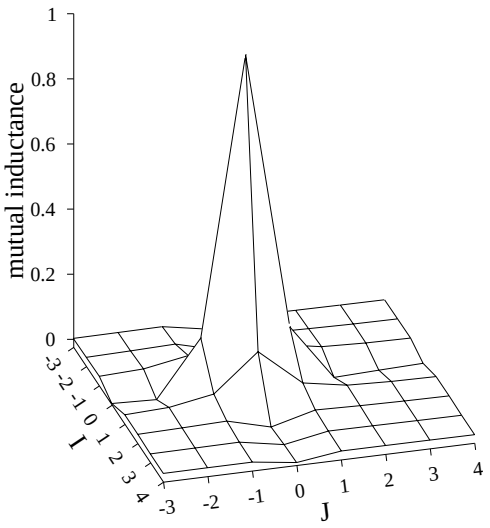

Fig. 2. Loop-loop mutual inductance *versus* loop distance. The ratio of the distance between the meshes and thickness of the wires is $R/a = 11$.

therefore we have set $R/a = 11$ in all the numerical calculation (corresponding to an empty hole 10 times larger than the width of the films).

Under these approximations, the mutual inductance between the branches k and n is given by the Neumann formula

$$L_{\mathrm{b}}^{k,n} = \frac{\mu_0}{4\pi} \int_k \int_n \frac{\mathrm{d}\boldsymbol{s}_k \cdot \mathrm{d}\boldsymbol{s}_n}{r_{k,n}}. \tag{11}$$

A trivial simplification is that the only non-zero contributions are given by the branches lying on parallel lines.

The mutual inductance between two vertical branches, whose coordinates are IR apart along x and JR apart along y, thus reads

$$L_{\mathrm{b}I,J}^{\mathrm{VV}} = \frac{\mu_0}{4\pi} \int_0^R \mathrm{d}y \int_0^R \mathrm{d}y' \frac{1}{\sqrt{(y'-y+JR)^2+(IR)^2}}. \tag{12}$$

The integral can be explicitly evaluated:

$$L_{\mathrm{b}I,J}^{\mathrm{VV}} = \frac{\mu_0 R}{4\pi} \left[F(J+1,I) - 2F(J,I) + F(J-1,I)\right] \tag{13}$$

where we have defined the function $F(J,I)$ as:

$$F(J,I) \equiv J + (\sinh^{-1})(\frac{\mathrm{J}}{\mathrm{I}}) - \sqrt{(\mathrm{J}^2+\mathrm{I}^2)}. \tag{14}$$

For the mutual inductance of the horizontal branches the formula is the same with I and J interchanged. We recall that for $I = J = 0$ (coinciding loops) we use instead equation (9) or equation (10).

The amplitude of the mutual inductance terms (in L' units) as a function of the I and J coordinates (that count the number of cells between the cell were the screening current is circulating and the other cells) is shown in Figure 2.

We note that for the values we used the non-diagonal terms (*i.e.* the terms not considered in the NS approach) are always less than 14% of the main contribution.

3 Shapiro steps amplitude of dc-SQUID driven by an rf signal

The amplitude of the phase-locked region of the steps as a function of the other parameters of the system are an important piece of information. Until now the effects of the inductance parameter β_{L} have not yet been completely addressed. Preliminary results can be obtained from the analysis of the SQUID. For a SQUID in the overdamped limit the equations are obtained using the same procedure as above, in normalized units [19]:

$$\dot{\phi_1} + \sin\phi_1 = \gamma - \frac{1}{\beta_{\mathrm{L}}}(\phi_2 - \phi_1) + \frac{2\pi}{\beta_{\mathrm{L}}} f, \tag{15}$$

$$\dot{\phi_2} + \sin\phi_2 = \gamma + \frac{1}{\beta_{\mathrm{L}}}(\phi_2 - \phi_1) - \frac{2\pi}{\beta_{\mathrm{L}}} f. \tag{16}$$

where the term γ includes both the dc and ac driving current with normalized frequency ω, see equation (3). The sum and difference of the two equations are:

$$(\dot{\phi_2} + \dot{\phi_1}) + \sin\phi_2 + \sin\phi_1 = 2\gamma, \tag{17}$$

$$(\dot{\phi_2} - \dot{\phi_1}) + \sin\phi_2 - \sin\phi_1 = \frac{2}{\beta_{\mathrm{L}}}(\phi_2 - \phi_1) - \frac{4\pi}{\beta_{\mathrm{L}}} f. \tag{18}$$

For $f = 0$, equation (18) is an autonomous damped equation that admits the solution $\phi_1 = \phi_2$. Inserting this symmetry in the first equation, each junction of the SQUID obeys the equation of the single rf-driven single junction, and therefore the amplitude of the rf-induced steps does not depend on the inductive coupling β_{L}. In the limit of loosely coupled junctions (*i.e.* $\beta_{\mathrm{L}} \to \infty$) the left hand side of equation (18) vanishes, and one can assume $\phi_2 \simeq \phi_1$. Also for the rigid limit, $\beta_{\mathrm{L}}, \to 0$ the solution with almost identical phases in the two junctions is the only solution to prevent the left hand side of equation (18) from diverging, and therefore the behavior of the SQUID is analogous to the single junction case. One could conclude that also for larger arrays, in both limits of very small and very large β_{L}, the phases should be synchronized, no screening current develops in the system, and as far as the amplitude of the Shapiro steps is concerned, the arrays are identical to the single junction. In fact for the case of finite β_{L}, numerical simulations [7] have shown that in the overdamped limit the screening currents are always negligible, and this results is valid also for arrays modeled with the nearest neighbor approximation of the matrix $\hat{L}$. This result might be a consequence of the special symmetry of the equation that prevents the screening current from appearing. When mutual inductance effects are included the equations are not anymore symmetrical: a junction close to the border will experience a different field because the magnetic field due to the currents flowing

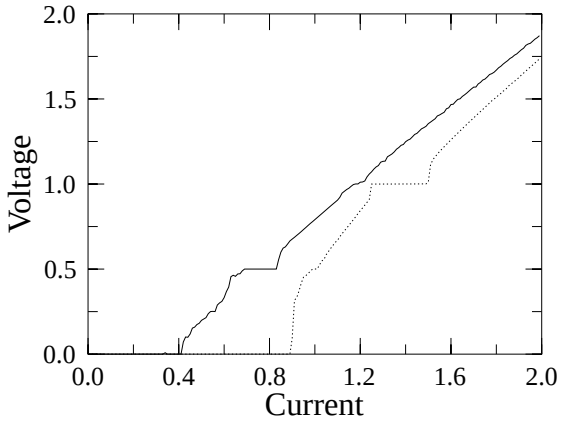

Fig. 3. IV curve for a square 8×8 array. Parameters of the simulations are: $\omega = 1$, $\beta_{\rm L} = 1$, $f = 0$ (dotted line) and $f = 1/2$ (solid line).

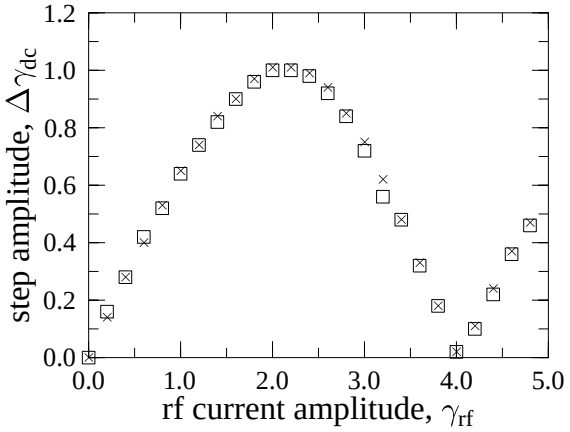

Fig. 4. Amplitude of the Shapiro step at the fundamental frequency *versus* the rf current amplitude $\gamma_{\rm rf}$ for a rigid 8×8 array described by equation (7) (□) and the NS equivalent equations (×). Parameters of the simulations are: $\omega = 1$, $\beta_{\rm L} = 0.1$, $f = 0$.

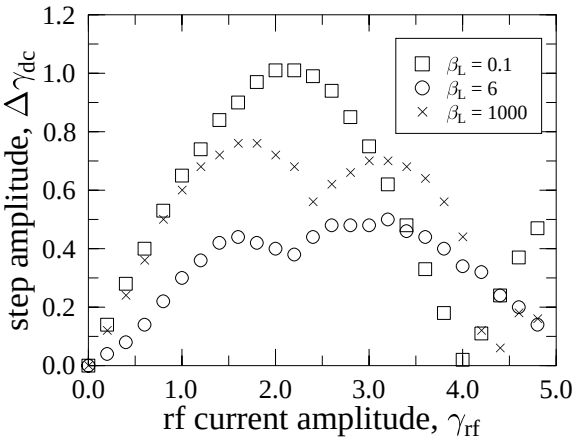

Fig. 5. Amplitude of the Shapiro step at the fundamental frequency *versus* the rf current amplitude $\gamma_{\rm rf}$ for a square 8×8 array. Parameters of the simulations are: $\omega = 1$, $f = 0$, $\beta_{\rm L} = 0.1$ (□), 6 (◯), 1000 (×).

on the left hand side will be larger than the field (of opposite direction) due to the currents flowing on the right hand side. To make quantitative this argument we have simulated equation (7) for different values of $\beta_{\rm L}$ and different fields. The results are shown in the next section.

4 Numerical Results

We have integrated equation (7), using the mutual inductance matrix described in Section 2 with $R/a = 11$. We will here show the results for the frequency of the external drive $\omega = 1$, similar results have been obtained also for higher values of the frequency. The dynamics showed no significant qualitative changes for arrays larger than 6×6, up to 12×12 arrays. As considerably long integration times arose increasing the array size, we show the results for a square 8×8 array. For the integration we used a fourth order Runge-Kutta method; usual transient time and voltage average time were $t = 400$ (normalized units), we have used $t = 0.05$ as integration step; in the stiff limits, such as for small $\beta_{\rm L}$, we have used shorter time steps and longer transient times.

In Figure 3 we show the IV curves for an 8×8 array to depict the qualitative behavior, also in presence of magnetic field. The effect of the rf term results in zero resistance branches called Shapiro steps. In the curves are clear both the fundamental step and the appearance of subharmonic steps. In this work we will focus on the steps appearing at the fundamental frequency, *i.e.* at voltage ω (in normalized units).

First, we have checked that in the rigid chain limit ($\beta_{\rm L} \to 0$) the full inductance model of the array described by equation (7) is well approximated by the nearest neighbor inductance model, or the NS model. In Figure 4 we show the zero field amplitude of the steps *versus* the rf-current $\gamma_{\rm rf}$, we chose $\beta_{\rm L} = 0.1$, and $\omega = 1$; circles and squares are the results for the model of equation (7) and the NS model. The two patterns are very close, thus confirming that the two models give the same results when $\beta_{\rm L} \to 0$. This is but a consequence of the fact that the self-field effects are negligible in the small $\beta_{\rm L}$ limit. Similarly, the Bessel-like structure is in agreement with previously analyses of the XY model [12,25].

In Figure 5 we show the Shapiro steps amplitude, $\Delta\gamma_{\rm dc}$, *versus* the value of the rf-current, $\gamma_{\rm rf}$, for three different β_y (the other parameters are: 8×8 array, $\omega = 1$, $f = 0$): it is clear that the Bessel-function behavior, typical of the rigid limit $\beta_L \to 0$, disappears for weaker coupling and a double maxima curve appears. The lower step amplitude for higher β_L is due to the progressive decoupling of the individual junctions, as will be explained below. For still higher $\beta_{\rm L}$ the results tend again to the Bessel-type curve.

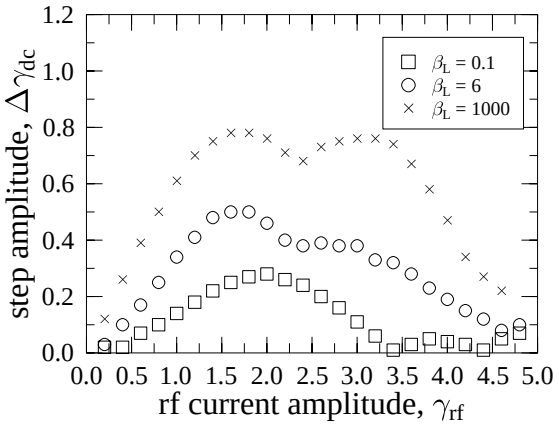

Fig. 6. Amplitude of the Shapiro step at the fundamental frequency *versus* the rf current amplitude $\gamma_{\rm rf}$ for a square 8×8 array. Parameters of the simulations are: $\omega = 1$, $f = 1/2$, $\beta_{\rm L} = 0.1$ (□), 6 (◯), 1000 (×).

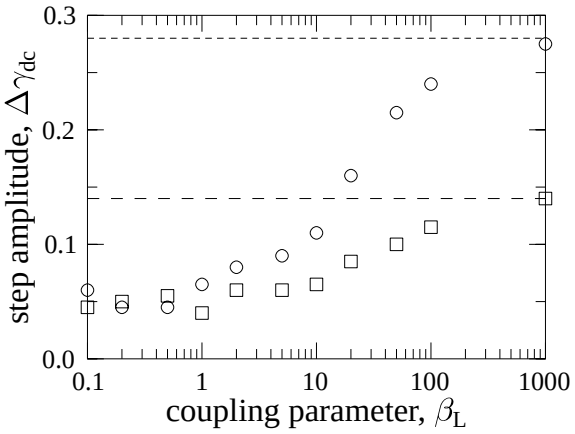

Fig. 8. Amplitude of the Shapiro step at the fundamental frequency *versus* the coupling term $\beta_{\rm L}$ for a square 8×8 array. Parameters of the simulations are $f = 1/2$, $\omega = 1$, $\gamma_{\rm rf} = 0.2(\square),\ 0.4(\bigcirc)$.

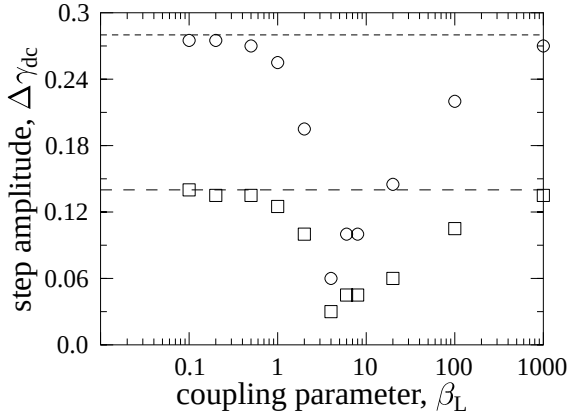

Fig. 7. Amplitude of the Shapiro step at the fundamental frequency *versus* the coupling term $\beta_{\rm L}$ for a square 8×8 array. Parameters of the simulations are: $f = 0$, $\omega = 1$, $\gamma_{\rm rf} = 0.2(\square),\ 0.4(\bigcirc)$. The lines correspond to the analytical prediction of reference [25].

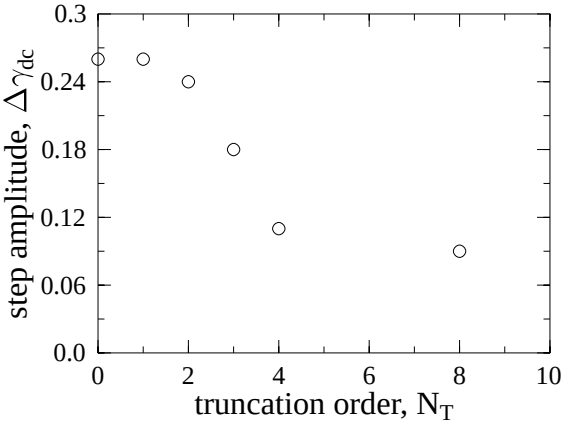

Fig. 9. Amplitude of the Shapiro step at the fundamental frequency *versus* the order of truncation of the mutual inductance matrix for a square 8×8 array. $N_{\rm T} = 0$ corresponds to the Nakajima-Sawada model, $N_{\rm T} = 8$ represents the full inductance matrix for this array size. Parameters of the simulations are: $f = 0$, $\omega = 1$, $\beta_{\rm L} = 6$; $\gamma_{\rm rf} = 0.4$.

Figure 6 shows a similar behavior for the fully frustrated case ($f = 1/2$). Here a double bump arises also in the rigid limit. Moreover, the Shapiro steps becomes smaller decreasing the $\beta_{\rm L}$ parameter. Inspection of the IV curve showed that this is due to the contemporary presence of subharmonic steps.

In the above figures we see smaller amplitudes of the Shapiro steps for intermediate couplings and zero field, while we have observed a monotone behavior for the fully frustrated case. We underline this behavior in Figures 7 and 8, where we show the Shapiro steps amplitude varying $\beta_{\rm L}$ for two rf current amplitudes $\gamma_{\rm rf} = 0.2,\ 0.4$ (to check that we are still in the linear regime and we can apply the analysis carried out in Ref. [25]) and for fixed frequency $\omega = 1$. Let us begin our analysis from the unfrustrated case $f = 0$, Figure 7. The amplitude of the Shapiro steps in the limits of very large and very small $\beta_{\rm L}$ (the last one corresponding to the XY or NS limit) tends, within the accuracy of the numerical scheme, to the theoretical amplitude of the Shapiro steps of isolated junctions [25]. In between there is a minimum for $\beta_{\rm L} \simeq 5$. We have also performed simulations with another expression for the self inductance, equation (10); In this case the minimum appears at higher value of $\beta_{\rm L}$, namely $\beta_L \simeq 8$.

We have also checked that this minimum is peculiar of the models with mutual inductance terms and is not observed simulating the simpler NS model or next-neighbor model. A check with truncated inductance matrix, for the array dimensions used here, shows that to clearly observe

the minimum at least a third order in truncated matrix formulation is necessary. This can be viewed in Figure 9 where the height of step for $\beta_{\rm L} = 6$ and $\gamma_{\rm rf} = 0.4$ is reported for different truncated matrix in the 8×8 array. In this figure the zero-order truncation corresponds to the NS model, $N_{\rm T} = 1$ represents the next-neighbor model, $N_{\rm T} = 2$ the next-next-neighbor and so on. Finally, $N_{\rm T} = 8$ is the full matrix model for this array size. We have checked, simulating the current distribution in the array, that the results are similar to that denoted as "case i" in Appendix C of [20]. From Figure 9 one can conclude that a 30% decrease of the Shapiro step occurs only when $N_{\rm T} = 3$. We have also simulated a larger array, $N_{\rm r} = N_{\rm c} = 11$; in this case the Shapiro step decreases of 27% at $N_{\rm T} = 3$.

The minimum can be explained in terms of the internal degree of freedom arising in this region of the parameters: For high couplings the array is too rigid for any internal dynamics thus giving a single junction behavior. A progressive loss of correlation appears for lower couplings, until in the very loose limit every phase is independent of the others, giving larger steps.

In Figure 8 we show the behavior of the fully frustrated case $f = 1/2$. In this case the amplitude is small for the high coupling limit, and increases for lower coupling until it reaches an asymptotic value. The reduced amplitude of the step for low $\beta_{\rm L}$ is due to the presence of a fractional step at frequency $\omega/2$. Indeed, while the amplitude of subharmonic steps is almost always negligible in zero field, it becomes relevant for $f = 1/2$ in the $\beta_L \to 0$ limit. This contribution has been explicitly calculated for $\beta_L = 0$ [12], it can be explained by the synchronization of the field generated pattern with the rf current. The subharmonic steps amplitude goes always to zero for loose coupling, therefore for the fully frustrated case the mutual inductance terms do not significantly change the overall picture.

To obtain further insight on the internal dynamics we have plotted in Figure 10 the voltage across side vertical junctions in the first four rows (the pattern is symmetrical for the remaining four rows in 8×8 array) at the center of the phase-locked step. First we have checked that for small values of $\beta_{\rm L}$ the voltage oscillations are practically the same for all the junctions in the array and have all the same phase respect to the drive due to the rigidity imposed to array by a large coupling, $1/\beta_{\rm L} \to \infty$. We begin our investigation by the intermediate coupling, as in Figure 10a, where we have set $\beta_{\rm L} = 6$. The inner rows (◯, ×, □) are phase-locked, but not in-phase. Moreover, the amplitude of the oscillations in the four rows is practically the same. In Figure 10b (the loose coupling limit, $\beta_{\rm L} = 1000$) inner rows (◯, ×, □) are phase-locked (but not in-phase) and voltage waveforms are very similar. This is not the case for the first row (◇): The voltage amplitude is larger than others rows. We also note that spread in phases is larger for the case of Figure 10b than that of Figure 10a. In conclusion, increasing $\beta_{\rm L}$ above unity implies a loss of strictly coherent phase-locking between rows due to the weakness of the coupling. For larger values of $\beta_{\rm L}$ a further progressive decoupling between different rows appears due

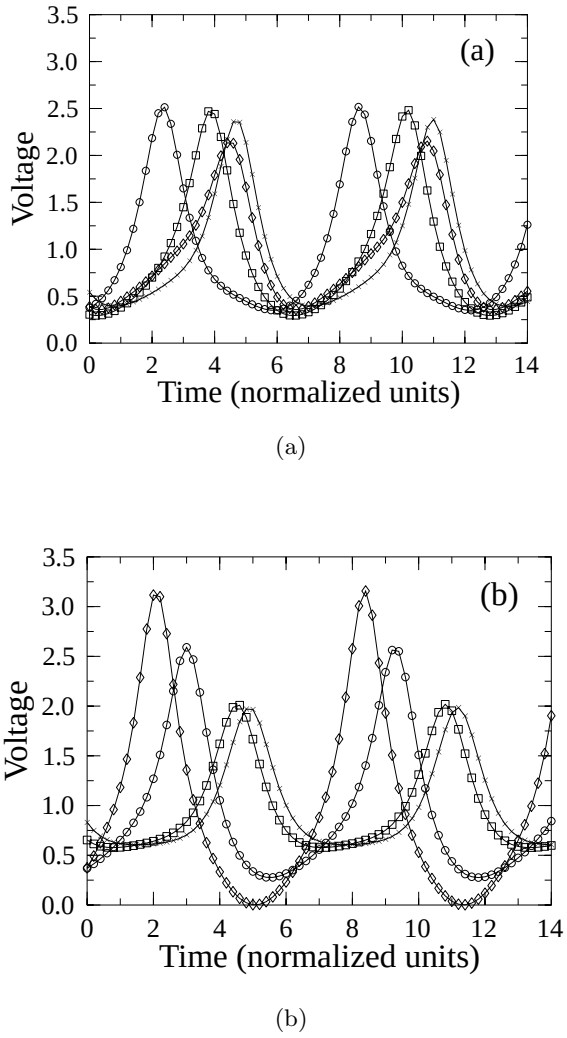

Fig. 10. Voltage oscillations of first four vertical junctions (first: ◇, second: ◯, third: □, fourth: ×) for a square 8×8 array. Parameters of the simulations are: a) $\beta_{\rm L} = 6$, $\omega = 1$, $\gamma_{\rm dc} = 1.35$; b) $\beta_{\rm L} = 1000$, $\omega = 1$, $\gamma_{\rm dc} = 1.4$. The dc bias has been changed to bias the array always at the middle of the step.

to the spread of both phases and amplitudes. The behavior of the amplitude of the Shapiro steps indicates that in the large $\beta_{\rm L}$ limit the first rows of the array support the larger oscillations.

To summarize this section, let us emphasize that the analysis of the Shapiro steps amplitude just carried out completes the one depicted by Phillips *et al.* in reference [15] for zero magnetic field. In reference [15] (see Fig. (5c)) a scaling law for $\Delta\gamma$ *vs.* $N\beta_{\rm L}$ (the parameter $\lambda_\perp = \Phi_0/2\pi I_0 \mu_0 R$ used in the referred work is inversely proportional to $\beta_{\rm L}$, and is roughly the penetration depth of the magnetic field) is shown, corresponding to a range in which $\beta_{\rm L} < 2$ ($1 \leq \lambda_\perp \leq 5$). In fact using equation (9) one finds $\beta_{\rm L} \simeq \lambda_\perp^{-1}$ or, using equation (10), $\beta_{\rm L} \simeq 1.8\lambda_\perp^{-1}$. We claim here that for relatively small N and increasing

β_L above the values explored by Phillips *et al.* a new behavior is found. On the other hand it is clear that if a scaling law would hold for all the values of β_L, one should get zero amplitude Shapiro steps for decoupled junctions, which is obviously not the case. In the present paper we have not investigated the behavior for larger sizes, we can only speculate that in the case of larger arrays the minimum might move to still higher β_L values, and the behavior here described can be very well compatible with the scaling law observed in reference [15] for moderately low values of $\lambda_\perp$.

5 Conclusions

In this work we have addressed the role of the inductances in relatively small two-dimensional arrays of Josephson junctions. We have included mutual inductance effects with an explicit scheme that is very efficient from a computational point of view for the systems sizes here considered and does not require the use of sophisticated algorithms to accelerate the convergence [15]. We have performed extended simulations to investigate the role of the coupling parameter β_L on the amplitude of the rf-induced steps in a range not investigated by previous authors. We have found that in this regime the amplitude of the steps of unfrustrated arrays decreases monotonically increasing β_L from 0 (the XY limit) to the maximum value investigated so far ($\beta_L \simeq 1$); increasing further β_L the amplitude of the steps reaches a minimum for $\beta_L \simeq 6$ and then increases again up to the XY limit value. This behavior is plausible on the basis of some heuristic arguments, essentially based on the idea that an extremely rigid array behaves as a single junction, and so does also a very loose coupling array. We have not been able to analytically predict neither the β_L value for which the minimum should occur neither the minimal height of the Shapiro steps. Another interesting feature, that presumably makes an analytical insight very difficult, is that the presence of a minimum is due to the mutual inductance terms. For β_L values above such minimum the dynamics of the junctions belonging to internal rows is different from the behavior of the junctions on the edge. We expect that the inspection of the dynamics of the individual junctions could be the starting point for an analytical insight. For the fully frustrated case we have found a more regular behavior, that does not differ significantly from the behavior predicted by models that neglect mutual inductance terms.

Finally, we would like to speculate that some of the results presented here could be used to identify an appropriate range of parameters to achieve spontaneous phase-locking of Josephson junctions arrays. In fact it might be expected that when the parameters are such that large amplitude Shapiro steps appear, also internal phase-locking mechanisms could be more efficient. If this could be proved, then we might suggest that arrays with small inductance ($\beta_L < 1$) are preferably to achieve the synchronous motion of the junctions in the array, a dynamics desirable for applications of Josephson junctions arrays as microwave sources [26].

This work was encouraged in an early stage by R.D. Parmentier, who tragically died on January 2, 1997. We wish to thank P. Carelli, G. Costabile, C. De Leo, R. Kleiner, S. Pagano, and A. Ustinov for useful discussions and suggestions. A.P. wishes to thank the EU for financial support through the Structural Fund.

References

1. S.P. Benz, M.S. Rzchowski, M. Tinkham, C.J. Lobb, Phys. Rev. Lett. **64**, 693 (1990).
2. K.H. Lee, D. Stroud, J.S. Chung, Phys. Rev. Lett. **64**, 962 (1990).
3. M. Octavio *et al.*, Phys. Rev. B **44**, 4601 (1991).
4. L.L. Sohn *et al.*, Phys. Rev. B **45**, 3003 (1992).
5. D. Domínguez, V. José, Int. J. Mod. Phys. B **8**, 3749 (1994).
6. M.S. Rzchowski, L.L. Sohn, M. Tinkham, Phys. Rev. B **43**, 8682 (1991).
7. A. Petraglia, G. Filatrella, G. Rotoli, Phys. Rev. B **53**, 2732 (1996).
8. K. Nakajima, Y. Sawada, J. Appl. Phys. **52**, 5732 (1981).
9. K.H. Lee, D. Stroud, Phys. Rev. B **43**, 5280 (1991).
10. H.C. Lee *et al.*, Phys. Rev. B **44**, 921 (1991).
11. S.E. Hebboul, J.C. Garland, Phys. Rev. B **47**, 5190 (1993).
12. I.F. Marino, Phys. Rev. B **52**, 6775 (1995).
13. A. Majhofer, T. Wolf, W. Dieterich, Phys. Rev. B **44**, 9634 (1991).
14. D. Reinel, V. Dieterich, T. Wolf, A. Majhofer, Phys. Rev. B **49**, 9118 (1994).
15. J.R. Phillips, H.S.J.V. der Zant, J. White, T.P. Orlando, Phys. Rev. B **50**, 9387 (1994).
16. C. Vanneste *et al.*, J. Appl. Phys. **64**, 242 (1988).
17. S.G. Lachenmann, T. Doderer, R.P. Huebener, T.J. Hagenaars, J.E. von Himbergen, P.H.E. Tiesinga, J.V. Jose, Phys. Rev. B **56**, 5564 (1997).
18. C. Lucheroni, Phys. Rev. B **55**, 6559 (1997).
19. A. Barone, G. Paternò, *Physics and Applications of the Josephson effect* (J. Wiley and Sons, New York, 1982).
20. D. Domínguez, V. José, Phys. Rev. B **53**, 11692 (1996).
21. J.R. Phillips, H.S.J.V. der Zant, J. White, T.P. Orlando, Phys. Rev. B **47**, 5219 (1993).
22. R.W. King, *Handbuch der Physik*, Vol. XVI, (Springer-Verlag, Berlin, 1958), p.197.
23. P. Carelli, M.G. Castellano, R. Leoni, Curr. Top. Magn. Res. **1**, 159 (1994).
24. A.E. Ruehli, IBM J. Res. Develop. **16**, 470 (1972).
25. N. Grønbech-Jensen, M.R. Samuelsen, Phys. Lett. A **191**, 57 (1994).
26. P.A.A. Booi, S.P. Benz, Appl. Phys. Lett. **64**, 2163 (1994).